A Study of Future Measurements of W Boson Helicity in $t \to Wb$ at CDF

Brock Tweedie

Advisor: Kevin McFarland

19 February 2002

Submitted in Partial Fulfillment of the Requirements for the Degree of
Bachelor of Science at the University of Rochester

Abstract

The interactions of the top quark will soon be coming under greater scrutiny at CDF with Run II of the Fermilab Tevatron collider. This investigation gauges CDF's improved ability to measure the helicity of W bosons produced in top quark decays. Such measurements will provide a direct indication of the spin structure of the weak interaction responsible for the top decay process. Simulated CDF Run II data is used to study the W helicity sensitivity of the muon momentum in μ+jets events, as limited by both statistical and systematic uncertainties. Optimization of helicity measurements via appropriate choices of event variables and data criteria is also addressed.

Contents

1 Introduction

1.1 The top quark

The 1995 discovery of the top (t) quark at Fermilab's Tevatron collider[1] [1][2] was in one respect less a surprise than a relief. Particle physicists had "known" that it was there ever since the discovery of the bottom (b) quark in 1977 [3], and had been anticipating both discoveries thanks to hints from earlier experiments [4][5]. Without a top quark, the relatively simple, if somewhat baffling, patterns of the intrinsic particle properties contained in the Standard Model of particle physics would fall just barely short of describing reality. Nature's seemingly arbitrary abandonment of those compelling patterns would have been too hard of a pill to swallow for most physicists.

But amidst the patterns of the Standard Model there are a few places where physicists must lend nature creative license. Most prominent are the particle's intrinsic energies, i.e. masses, which exist as experimentally determined parameters in the theory. In this respect, the top quark was guaranteed to be surprising, since no one could predict its mass.

And what a surprise that mass turned out to be. At around 175 GeV/c^2, top outweighs all of the other types of fermions put together by about a factor of 20, and is the only fermion more massive than the weak vector bosons. Not only is this mass abnormally large, it is abnormally large *enough* that the energy bound up inside the top quark is on par with the energy scale at which the electromagnetic and weak forces are thought to undergo unification. In fact, top's mass is equal to the unification theory's scaling parameter to within at most a few percent, raising it from abnormal to downright suspicious.

Physicists, eyebrows now thoroughly raised, are hoping that top will open up a new

[1] In its collider mode, the Tevatron collides oppositely-circulating beams of protons and antiprotons with energies of ~1 TeV per particle.

realm of physical phenomena for their study. For all of its success, no one seriously believes that the current Standard Model is the final say in particle theories, in large part because it fails to give a satisfying explanation of the observed pattern of particle masses. If there is in fact some unknown mechanism generating this pattern, then top seems to be on very intimate terms with it, and top's behavior will perhaps display some additional "oddities" indicating its influence. In addition, this mechanism would be related to the still-mysterious electroweak unification, to which top has already been shown to have some other interesting circumstantial connections.

1.2 The physics under study

Top lives for about 10^{-24}s, after which it decays with almost 100% probability into a bottom quark and a W boson via the weak interaction. Top's lifetime is so short that its decay is not influenced by strong force interactions. Consequently, the spins of the decay products serve as direct indications of the physics of the top quark's weak decay. The Standard Model makes some very definite predictions for these spins, so if top is indeed harboring "new physics," especially related to the weak force, then this is a prime place for that physics to be discovered.

When talking about spin, it is necessary to specify both a frame of reference and an axis. Here, as throughout the paper, the top's rest frame will serve as the frame of reference, unless otherwise stated, and a particle's direction of motion will serve as its spin axis. Spin measured along such an axis (regardless of the reference frame) is often called "helicity," and this convention will also be followed. Spin-$\frac{1}{2}$ fermions like bottom have only two possible helicities, $(+)$ and $(-)$, while massive spin-1 bosons like the W can also have (0) helicity. Figure 1 illustrates the helicity of the W and the bottom quark in the top quark rest frame.

In the Standard Model, charged weak interactions such as the top's decay have a built-in left-right asymmetry that manifests itself in the helicities of the particles produced. The asymmetry is "maximal" for massless fermions in the sense that either the $(+)$ or the $(-)$ helicity state is produced to exclusion. The general trend for all particles is favoritism of $(-)$ helicity for "normal" matter and $(+)$ helicity for antimatter. The quantitative degree of this favoritism has always been observed to be equal between matter and antimatter,

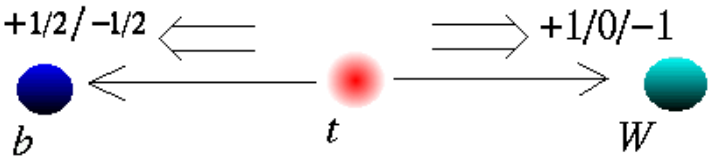

Figure 1: Helicities in the top rest frame. The single arrows indicate the directions of motion of top's decay products. The double arrows indicate the directions in which their spins are measured, and the numbers indicate possible values of the spin in units of $\hbar$. The spins get the label "helicity" because they are measured in the same directions that the respective particles are moving in.

indicating a combined charge-parity symmetry for these processes.[2] In the specific case of the top decay, this means that the products of the process $t \to W^+b$, and its antimatter analog $\overline{t} \to W^-\overline{b}$, should display equal and opposite helicities. This will be assumed in what follows, and further mention of top, its decay products, or the helicities of those products will implicitly refer to both the matter and antimatter cases but use the charge and spin conventions appropriate for the former.

Since the bottom quark has a mass of $\sim$5 GeV/c^2 and the energy scale of the top decay is $\sim$175 GeV/c^2, it is reasonable to treat bottom as "nearly-massless" in this process. From the discussion above, it is clear that if the Standard Model is correct, then the $(-)$ helicity will dominate. In fact, the $(+)$ helicity state of the bottom quark is predicted to be so rare in this decay that it can be treated as if it never occurs.[3] In the presence of only $(-)$ helicity bottom quarks, the W cannot have $(+)$ helicity either. A $(+)$ helicity W with a $(-)$ helicity bottom quark would imply a total spin of $+\frac{3}{2}$ to the right in Figure 1, which violates angular momentum conservation because the top quark is a spin-$\frac{1}{2}$ particle. The fractions of Ws exhibiting the remaining helicity states, (0) and $(-)$, are then specified by some slightly more complicated arguments involving the specific form of the standard weak force interaction [6]. Numerically at part per mil precision, the Standard Model values of the fractional occurrences of each helicity state for both the bottom quark and the W boson

[2]This symmetry is shown not to be an exact law of nature in Reference [5], but any violation in top decay is expected to be negligible for the purposes of this study.

[3]The $(+)$ helicity state is suppressed by factors on the order of $\frac{m_b^2}{m_W^2} = 0.003$.

are as follows:

$$\begin{aligned} f_+(b) &= 0.000 \\ f_-(b) &= 1.000 \end{aligned} \tag{1}$$

$$\begin{aligned} f_+(W) &= 0.000 \\ f_0(W) &= \frac{m_t^2}{2m_W^2 + m_t^2} = 0.701 \pm 0.012 \\ f_-(W) &= \frac{2m_W^2}{2m_W^2 + m_t^2} = 0.299 \pm 0.012 \end{aligned} \tag{2}$$

using the measured values of the top quark and W boson masses, 174.3 ± 5.1 GeV/c^2 and 80.4 ± 0.1 GeV/c^2, respectively [7].

The actual helicity fractions chosen by nature can be measured, with some important restrictions, by the same equipment used to discover top and measure its mass. Such measurements can then be used to check the validity of the Standard Model in the top decay process. The major point of interest here is to test whether the maximal parity asymmetry observed in all other charged weak interactions is still present in the case of the peculiar top quark. In other words, do $f_+(b)$ and $f_+(W)$ really equal 0 in $t \to Wb$?

1.3 Prospects for measuring helicities in $t \to Wb$

Unlike its parent top quark, the bottom quark produced in the decay *does* experience the strong force, as do most of its own decay products. The general result is a cascade of strongly-interacting particles dubbed a "jet," in which information on the bottom's original spin is completely lost. Measuring the helicity of the bottom quark is not an option.

The prospects for measuring the helicity of the W boson take a bit more work to classify. About 70% of the time, the W decays into a quark and an antiquark that form their own jets. However, the difficulty in determining which quark types produced which jets poses a major problem for extracting precise W helicity information from them, since the helicity can affect different quarks in opposite ways. 10% of the time, the W decays into a τ lepton and its neutrino. There are a variety of complications with this decay mode related to the τ's subsequent decay.[4] That leaves the other 20% of W decays, evenly distributed between

[4]The τ lepton has a variety of decay modes. Most of them are hadronic and hard to trace back to a

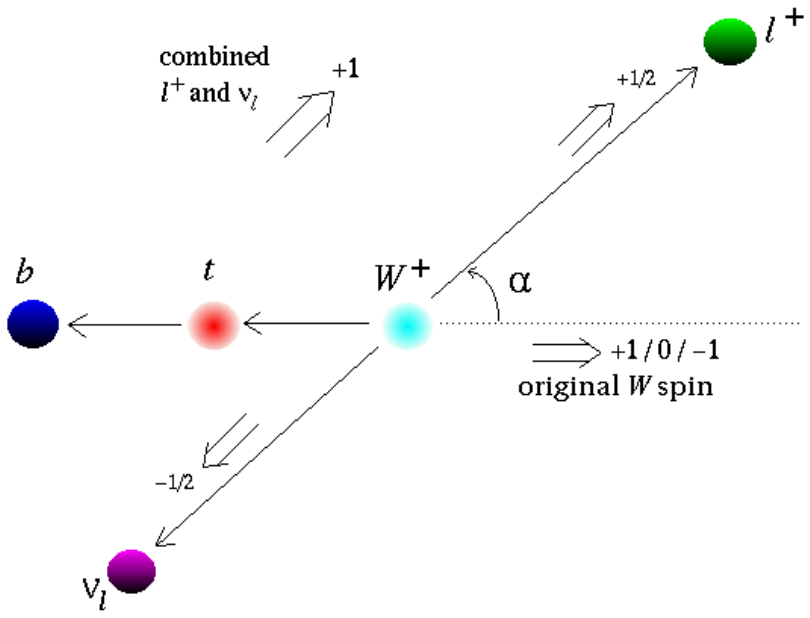

Figure 2: Spins in the W^+ rest frame. The W's helicity from the top frame is preserved as the spin in the right-hand direction. The helicities of the W's decay products are fixed by the weak force and constitute a $+1$ spin projection in the direction of the l^+, at polar angle α from the original spin axis.

decays into electrons or muons and their respective neutrinos, $W \to e\nu_e$ and $W \to \mu\nu_\mu$. The charged leptons produced in these decays are stable enough to be directly detected and identified. These leptonic W decay products are the most direct messengers of the W's helicity, and constitute the main resource for performing a precise measurment.[5]

The connection between the W's helicity and the W's decay products originates in the parity-violating helicity asymmetries discussed above. When a W decays into a charged lepton and its neutrino, any of which can be considered "nearly-massless" with respect to the W, the helicities of those products in the W's rest frame are almost exclusively negative for matter and almost exclusively positive for antimatter. For a W^+, this implies that the W has $+1$ spin along the charged lepton's direction of motion, as depicted in Figure 2. The W's top-frame spin axis and spin state are preserved in its own rest frame, so the probability

τ in the environment of $t\bar{t}$ decay. Regardless of the particular decay, the τ always produces at least one unobservable neutrino that carries away information.

[5]Since the fractions $f_{+/0/-}(W)$ have now been shown to be the relevant quantities for measurement, the distinguishing "(W)" label will be dropped in further references.

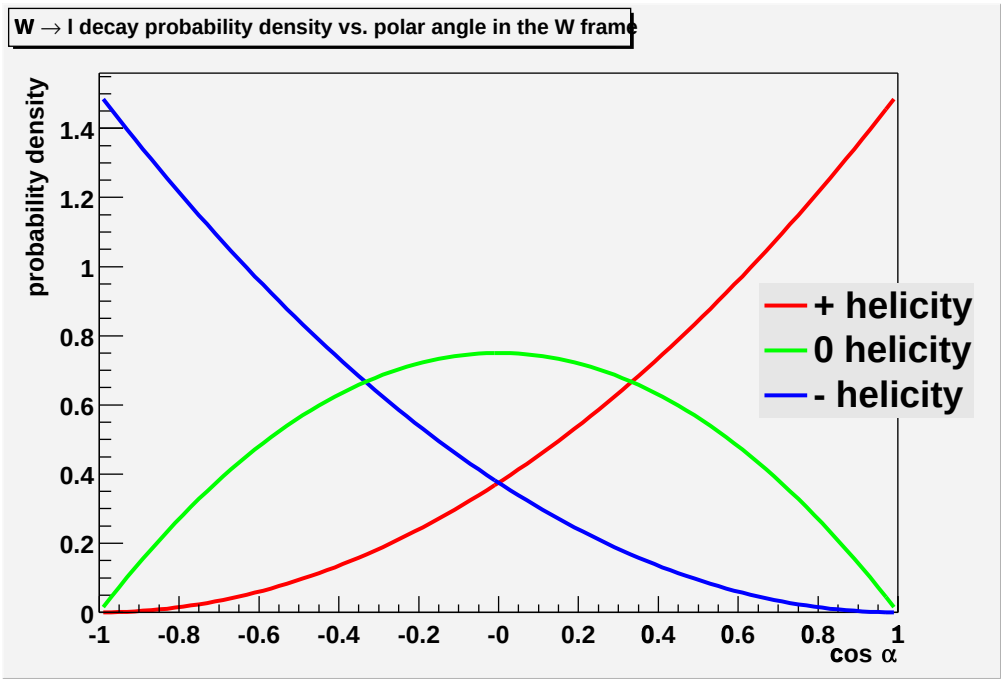

Figure 3: The lepton decay angle distributions for the three W helicities.

density, $\frac{d\mathcal{P}}{d(\cos\alpha)}$, of the charged lepton decay taking place at polar angle α from the original spin axis is modified by the probability of that state projecting a $+1$ value onto an axis at an angle α. For a W exhibiting one of the three helicity states, the decay angle distribution will be of one of the following forms:

$$\begin{aligned} \frac{d\mathcal{P}_+}{d(\cos\alpha)} &= \frac{3}{8}(1+\cos\alpha)^2 \\ \frac{d\mathcal{P}_0}{d(\cos\alpha)} &= \frac{3}{4}(1-\cos^2\alpha) \\ \frac{d\mathcal{P}_-}{d(\cos\alpha)} &= \frac{3}{8}(1-\cos\alpha)^2 \end{aligned} \tag{3}$$

These are graphed in Figure 3.

This kinematic dependence of the electrons and muons on the W's helicity is what makes that helicity measurable, since the effect carries over to variables that are directly observable in the lab. For example, if Ws produced in top decays at the Tevatron exhibited only one of the three helicities, then the momentum (P) distribution of the direct electrons and muons in the laboratory would exhibit one of the three characteristic shapes shown in Figure 4. Because (+) helicity Ws tend to decay into charged leptons with low α according to

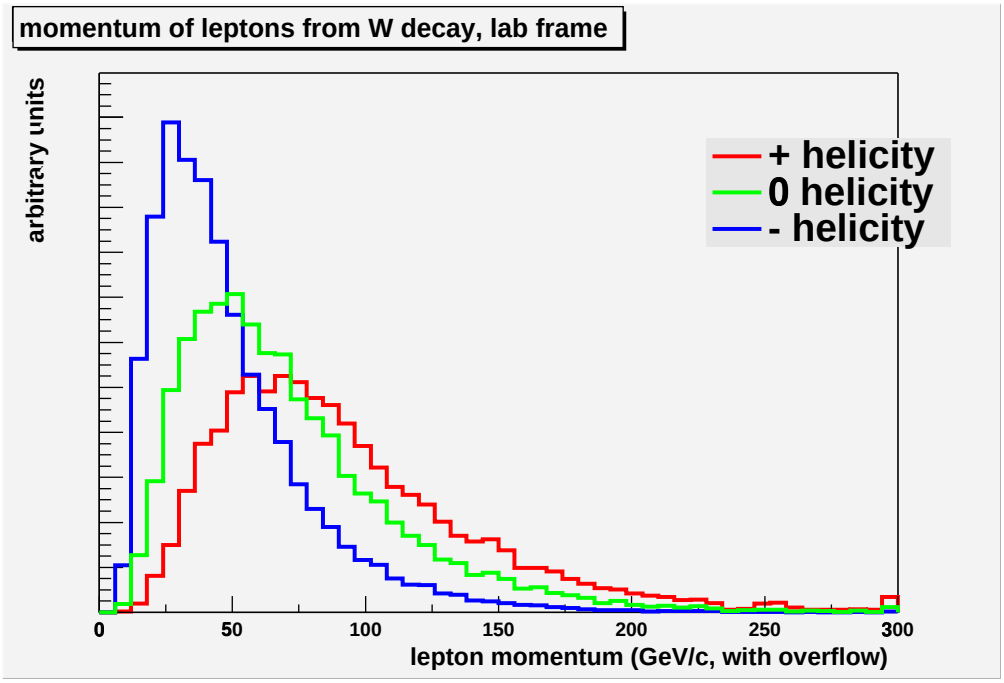

Figure 4: A distribution sensitive to W helicity.

Equations (3), and because low α corresponds to close alignment with the direction of the W in the top rest frame, the leptons produced tend to have higher momentum in that frame. Similarly, leptons from $(-)$ helicity Ws tend to have lower momentum and those from (0) helicity Ws are intermediate. The top is not produced at rest in the laboratory, but the effect persists in the lab frame as evidenced by the figure.

For the real sample of Ws produced from top decays, the helicity state is a quantum superposition of the three possible values. In general, such a superposition would be expected to produce nonlinear interference effects in variables sensitive to the W helicity, but they are expected to be negligible in this case [8]. Consequently, the distributions of those variables are actually simple linear superpositions where each helicity state is weighted by the fraction of Ws exhibiting it. The actual decay angle distribution is thus

$$\frac{d\mathcal{P}}{d(\cos\alpha)} = f_+ \frac{d\mathcal{P}_+}{d(\cos\alpha)} + f_0 \frac{d\mathcal{P}_0}{d(\cos\alpha)} + f_- \frac{d\mathcal{P}_-}{d(\cos\alpha)}, \tag{4}$$

and other distributions superimpose in the same manner, as illustrated in Figure 5. Measurement of the W helicity fractions therefore consists of observing the distribution of some variable sensitive to the helicity, calculating the single-helicity distributions in that variable, and

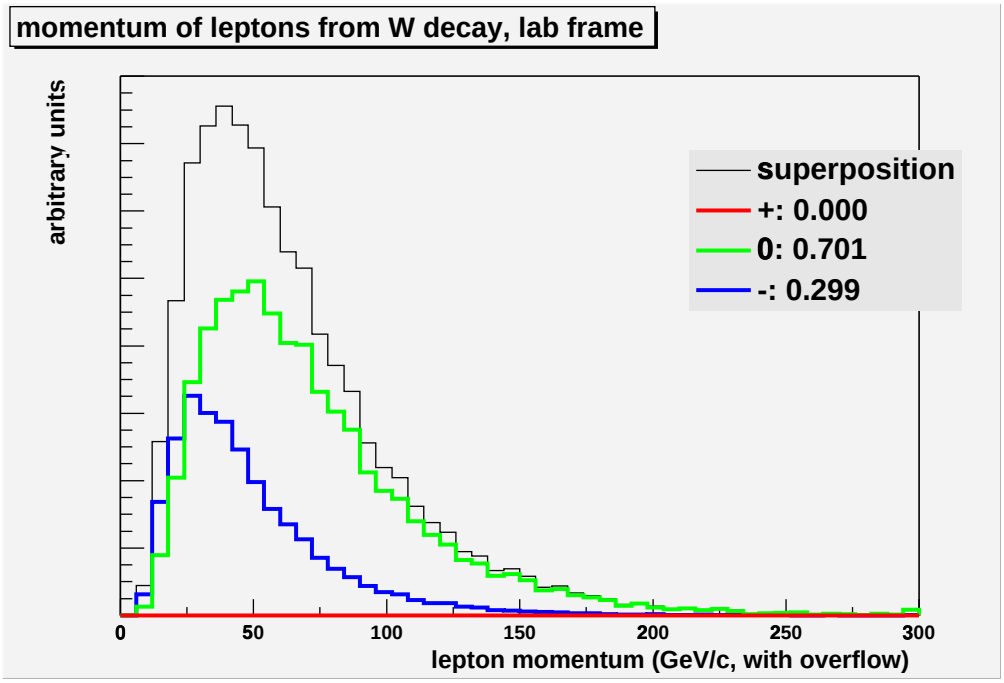

Figure 5: A superposition with Standard Model helicity fractions.

then finding the fractions (f_+, f_0, f_-) that produce the best linear fit to the data. Because $f_+ + f_0 + f_- = 1$, only two of the fractions need to be determined in the calculation, and the convention here will be to fit to (f_0, f_-).

1.4 The purpose and methodology of this study

In the first run of the Tevatron, in which the top quark was discovered, the Collider Detector Facility (CDF) collaboration performed the type of measurement described in the previous subsection [9]. The statistics were so low, however, that the measurement was completely inconclusive unless one of the fractions was assumed to be already known. With f_+ fixed to 0, representing the Standard Model's maximal helicity bias, the measurement yielded $f_0 = 0.91 \pm 0.39$. Though this result is consistent with the Standard Model physics responsible for the $f_0 = 0.70$ prediction, the size of the error does not make that consistency very compelling, nor does the measurement give any indication of the actual weak force helicity bias in the top's decay. With f_0 fixed to the Standard Model value 0.70, the measurement yielded $f_+ = 0.11 \pm 0.15$, which is again consistent with the Standard Model but not at all convincing of its applicability. (The result states that $f_+ < 0.28$ at the 95% confidence level,

when it is less than 0.30 by assumption.)

In March 2001, the Tevatron began an upgraded run (Run II) which, over the next several years, should provide the first large-scale sample of top quarks for detailed study. In anticipation of the new data that will be acquired, this paper makes preliminary estimates of the quality of several possible W helicity measurements that could be made by the CDF collaboration, with aim of detailing and minimizing the errors associated with those measurements.

The fundamental approach taken here is to make as realistic a facsimile of the Run II data set as possible, apply the measurement procedure introduced in Section 1.3 for a small sample of useful variables, and determine the errors on those measurements. Since the actual W helicity fractions are still essentially unmeasured, Standard Model physics has been assumed and "realistic" should be taken in the sense of representing what would actually be seen in the CDF detector under that physics.[6]

The study focuses exclusively on a subsample of the Run II data called "μ+jets." These are events where a $t\bar{t}$ pair is produced in the Tevatron and, upon the pair's decay into $(W^+b)(W^-\bar{b})$, one W subsequently decays into $\mu\nu_\mu$ and the other decays into hadrons. The choice to use just this subsample was based largely on time constraints. Different classes of events useful for W helicity measurements have different sources of error, and a thorough investigation of all of these sources was not possible over the course of this research. The μ+jets subsample was the natural place to start because it constitutes approximately half of the total useful data and is easier to fully analyze than the analogous and similarly-sized e+jets subsample, owing to extra detection issues associated with electrons. To estimate the quality of results that will be derived from the entire direct lepton data set, double-sized μ+jets samples are used. Pretending that e+jets electrons are actually muons has the effect of unnaturally increasing the quality of the simulated helicity measurements, but the failure to incorporate the final class of direct lepton events, "dilepton," more than offsets this, making the estimate a conservative one. Dilepton events are events where both Ws decay leptonically, and they will constitute the highest-quality $t\bar{t}$ subsample, though they

[6] Of course, if the values of the W helicity fractions are correlated with their measurement errors, and those fractions turn out to be highly nonstandard, then the estimates made here may be of limited use. However, such an extreme discrepancy between theory and reality is, to say the least, unlikely.

will only account for on the order of 10% of the observed direct leptons.

To introduce the experimental setting in which the W helicity measurements will be performed, and which this study attempts to simulate, the next section discusses the CDF detector in more detail. Section 3 then outlines the procedures by which simulated detector data is used to estimate the errors on the W helicity measurements. Sections 4 and 5 respectively report the statistical and systematic errors found for a small set of measurements, and Section 6 presents the optimized total errors. Finally, conclusions are presented in Section 7.

2 The CDF Detector

2.1 Components

The CDF detector is a hybrid of several different types of more basic detectors. The central body of the detector can be envisioned as a series of nested cylindrical regions containing the different detector components. At the very center is the beampipe, where high-energy protons and antiprotons provided by the Tevatron collide to make interesting things like top.

Immediately surrounding the beampipe is the Silicon Vertex Detector (SVX), consisting of layers of silicon trackers that are used to pinpoint the origins of particles' paths through the detector. One of its main purposes is to identify bottom quark jets, which often originate at a "displaced vertex" located on the order of a millimeter away from the primary vertex because of the bottom quark's relatively long lifetime.

The next layer of detector is the Central Outer Tracker (COT). This is a series of wire drift chambers, acting like thousands of localized Geiger counters that react to the passage of charged particles. The trail of wire "hits" left by a particle can be used to trace its path. A magnetic field applied parallel to the cylindrical axis bends particles' paths into helices, allowing for determination of both charge and momentum via measurement of the direction and magnitude of curvature. The tracking performed in the COT is supplemented by the SVX and vice-versa.

Electromagnetic and hadronic calorimeters surround the COT. Each consists of alternating layers of scintillator and absorbing material. Different types of particles are stopped in

the different calorimeters, where they deposit energy in the form of showers of secondary particles which are observed in the scintillators, allowing for measurement of that energy. The electromagnetic calorimeter is the innermost of the two calorimeters, and measures the energy from electrons and photons. High-energy hadrons, charged or otherwise, pass through the electromagnetic calorimeter relatively undisturbed and are stopped and measured by the hadronic calorimeter.

The outermost layer of the detector is the muon tracking system, responsible for identifying the particles used in this study. Muons almost never shower passing through matter, so most will fly right out of the CDF detector. The muon tracking system records the passage of particles that do just that, using a hodgepodge of drift chambers and other detectors mounted outside of several feet of steel detector housing. A track in the COT that can be traced outside of the detector and linked to muon tracking hits is considered a muon track.

Figure 6 shows a side-on cross-section schematic of the whole detector, including a few parts not explicitly under discussion. Figure 7 is an end-view photograph of the detector, with the SVX and an end plug full of calorimeters prepared for installation. Figure 8 shows an end-on cross-section view of a simulated event in the detector, illustrating the role of all of its major components.

2.2 Definitions of detector variables

CDF uses a spherical coordinate system for its detector, with the center of the system corresponding to the center of the detector. The azimuthal angle ϕ is defined in the plane perpendicular to the beampipe. The polar angle θ is defined with respect to the beampipe, which serves as the z-axis. Generally, θ is replaced by the pseudorapidity, $\eta \equiv -\ln(\tan\frac{\theta}{2})$. Pseudorapidity is a useful variable because particle flux in the detector is approximately uniformly distributed over it.

Because the detector is cylindrical, particle momenta are broken-down into parts transverse to and parallel to the beampipe, labeled P_T and P_z, respectively. For particles depositing energy in the calorimeters, the relevant quantity is transverse energy (E_T) which is the projection of energy onto the transverse plane as if it were a vector aligned with momentum. This quantity is more convenient than total energy for determining which calorimeter data

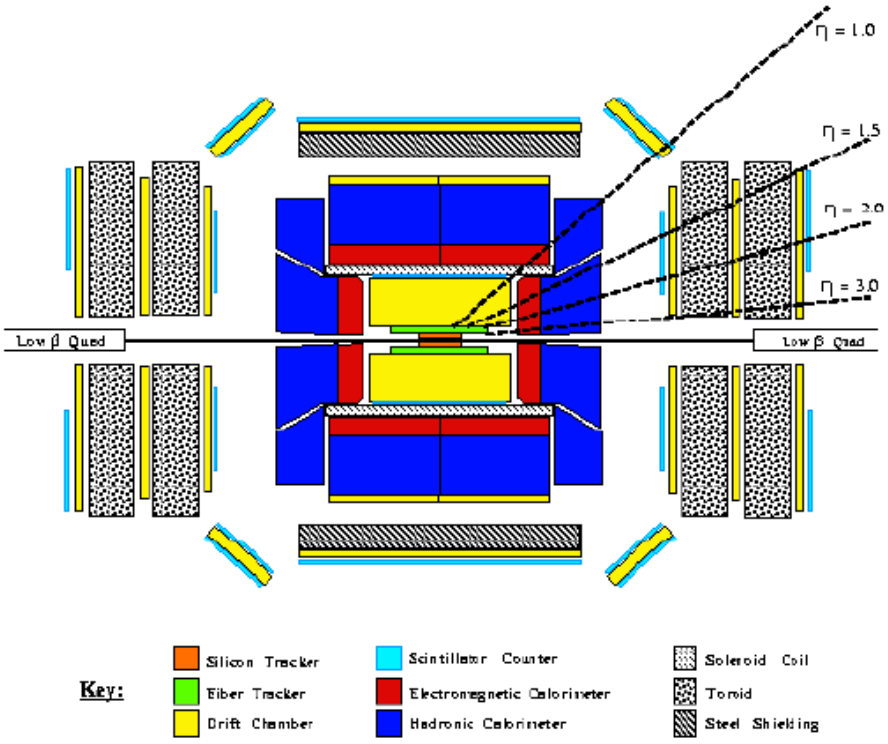

Figure 6: A side-on cross-section schematic of the Run II CDF detector. Rotation of the schematic about the beampipe (running horizontally through the center) traces out the detector's solid cylindrical structure.

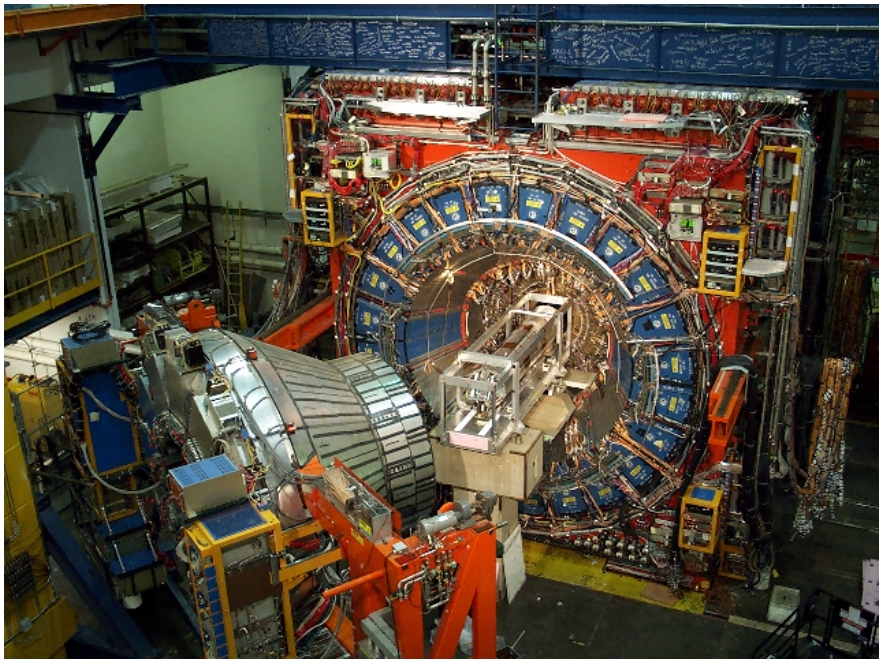

Figure 7: An end-on photograph of the CDF detector under construction.

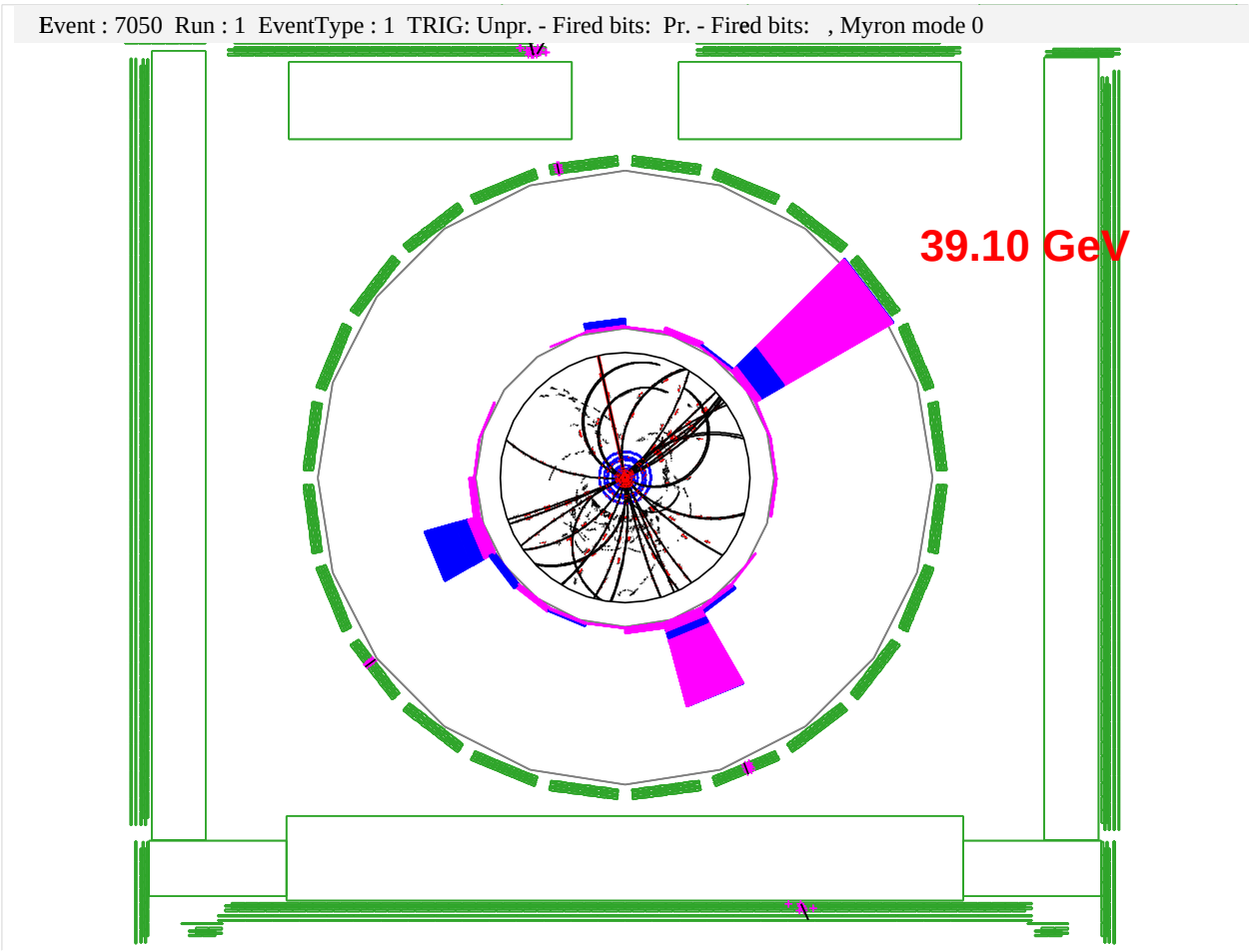

Figure 8: An end-on cross-sectional view of a simulated μ+jets event in the CDF detector. The SVX is the series of blue circles at the center, partially obscured by the red particle hits within it. The black arcs are tracks in the COT, reconstructed from both the wire hits and the silicon hits. The purple and blue wedges represent energy deposits in the calorimeters. The green regions are muon trackers, and the purple dots within them are particle hits. The hits near the top of the figure came from a muon that decayed off of a W, and the corresponding COT track can be easily found. The hits near the bottom right were left by a muon produced inside of a b jet (the one setting off the calorimeters there). The hits in the lower left segment of the inner muon tracker were not left by a muon, but by some other high-energy particle that managed to punch through to the outer part of the detector.

is potentially interesting, especially in the forward part of the detector.

Events generated by colliding beams generally take place with very little total transverse motion, so the products have momenta and E_T that balance out in the transverse plane. The CDF calorimetry is complete over ϕ and excludes only regions of very high $|\eta|$ (as indicated by Figure 6), occupied by the plethora of low-E_T collision debris that flies down the beampipe in each event. Since this low-angle debris part of the event has very small vector-summed E_T, so must the part of the event that passes through the detector in order to keep their sum at approximately 0. Hence, the vector sum of the *measured* transverse energy of an event should add up to almost 0 *unless* something is escaping detection in the calorimeters and muon trackers. This is exactly the case for neutrinos, and the "missing" E_T ($\not\!\!E_T$) necessary to bring an event into azimuthal balance can often be a signature of those particles.

3 Procedures for Simulating the Run II CDF Measurements

3.1 Generation of sample data

As the basis for the simulated W helicity measurements, ten samples of 14,000 $t\bar{t}$ events each are simulated using the HERWIG Monte Carlo package [10] under Standard Model physics with $m_t = 175$ GeV/c^2 and with the Run II center-of-mass beam energy of 2 TeV. The CDF detector response to these samples is also simulated and algorithms for event reconstruction and particle identification are applied.[7,8] The event depicted in Figure 8 is from these samples.

Since μ+jets events cannot be unambiguously identified by the detector, there are standard event selection criteria which, when applied to the set of all events recorded by CDF, are intended to weed out as much of everything else as possible. The criteria used in this study are as follows:

1. The event contains a track identified as a muon with 8 GeV/c $< P_T <$ 500 GeV/c and $|\eta| < 1.2$. The P_T cut removes very "soft" muons that are uncharacteristic of W decay,

[7] On 500MHz Pentium II processors, an average event took ~20s for the entire sequence of operations. Each event occupied ~300Kb of hard drive space.

[8] The percentage of muons identified here is not a highly accurate reflection of CDF's actual capabilities. The software identification rate is something in the ballpark of 20% less than what is actually anticipated.

as well as very high P_T tracks with curvature that is too low to accurately measure. The η cut is implicitly imposed by the coverage of the muon detectors.

2. The muon's P_T constitutes at least 90% of the scalar-summed P_T of all particles found within an η-ϕ cone of radius 0.35 about the muon's initial trajectory. This is intended to remove muons produced inside of hadronic jets by requiring isolated tracks.

3. The muon is the highest-P_T lepton in the event. Any other leptons with higher P_T are more likely to have come from a W.

4. $\not\!\!E_T > 20$ GeV, which usually indicates the presence of a high-energy neutrino produced in leptonic W decay.

5. There are at least three hadronic jets with $E_T > 15$ GeV and $|\eta| < 2.0$.

6. There is a fourth jet with $E_T > 8$ GeV and $|\eta| < 2.4$. Together, this criterion and the previous criterion ensure the jet structure characteristic of a $t\bar{t}$ event where one W decays hadronically.

7. At least one jet is tagged with a displaced vertex by the SVX, indicating the presence of one or more bottom quarks in the event.

For events passing all of the criteria, the muon of criteria (1)-(3) is considered the μ in μ+jets. Inevitably, some of the events that pass the criteria are not actually μ+jets. (The muon track does not even necessarily belong to an actual muon.) Since they are not useful for the measurement, such events are characterized as background.

When this study was performed, the CDF reconstruction software necessary to calculate $\not\!\!E_T$ had not been completed, so special care had to be taken to replicate the $\not\!\!E_T > 20$ GeV criterion. For events with leptons from W decays, the vector sum of Monte Carlo level neutrino P_T stands in for $\not\!\!E_T$. For events without leptons from W decays, called "non-W" events, no such procedure can be convincingly applied because those events would only realistically pass the $\not\!\!E_T$ criterion due to misreconstructions in the calorimetry. As a workaround, the events are simply weighted by a factor of 1.9 to match the relative non-W background fraction found in the Run I l+jets sample (where $l = \mu$ or e) [11]. This

procedure has the additional benefit of "including" non-W events from all processes, even though this Monte Carlo only generated them using $t\bar{t}$ events. Though the weighting is by no means a perfect substitute for an actual $\not\!\!E_T$ cut and an actual simulation of the non-$t\bar{t}$ non-W processes, the number of events is small and their general characteristics should be accurately reflected.

In addition to the unsimulated portion of the non-W background, there is one other major class of background events, called "W+jets," that is not represented in the simulated $t\bar{t}$ event samples. These include any non-$t\bar{t}$ processes that produce a W boson and hadronic jets. A very small fraction of W+jets events pass the μ+jets criteria when the W decays into a muon, either directly or via an intermediate τ. In fact, that fraction is so small that simulation of W+jets for the study (also using HERWIG) was complicated by the sheer number of events necessary to produce a sizable subsample that passes the selection criteria[9] (where, as with the other events containing leptonic W decays, the Monte Carlo neutrino P_T is used for the $\not\!\!E_T$ cut). The major difficulty in finding W+jets events that pass the μ+jets criteria is the rarity of the appropriate jet structure, so, to facilitate the inclusion of W+jets data in the study, the criteria (5) and (6) are replaced with the single, looser criterion "there are at least three hadronic jets with $\mathrm{E}_T > 8$ GeV and $|\eta| < 2.4$." This is meant to preserve at least the gross features of a sample of muons from non-$t\bar{t}$ Ws produced with four jets. The W+jets sample generated for the study contains 209 total events that pass the modified μ+jets criteria. These events are weighted by 0.38 to match the Run I W+jets:$t\bar{t}$ event ratio and introduced into the ten data samples with random fluctuations generated according to the Poisson probability distribution.

The final composition of the average μ+jets data sample, taking into account weightings, is

- 700 actual μ+jets events[10]
- 88 τ+jets events where the τ decayed into a muon

[9] Even with Monte Carlo level filtering that only passes events with $W \to \mu\nu_\mu$ and $W \to \tau\nu_\tau \to \mu\nu_\mu\nu_\tau\nu_\tau$, removing 90% of unwanted data at the outset, only about 1 in 1000 events passes the μ+jets criteria. Simulating enough W+jets events so that just 100 pass the criteria would require ~550 hours of processor time.

[10] This constitutes 57% of the total number of actual μ+jets events tracked in the simulated detector.

- 31 non-W events
- 78 W+jets events

The total size of the average sample, 897 events, is about double what is expected for μ+jets from the 2 fb^{-1} of integrated luminosity[11] in the first stage of Run II. Thus, the measurement errors associated with these samples will be representative of what will be seen for the entire direct lepton sample collected during this stage.

The influence of the three backgrounds (τ+jets, non-W, W+jets) on the measurements will be explored in Sections 4 through 6. The presence of the backgrounds in the combined ten samples is shown in Figure 9 for the muon P_T variable, and their shapes in that variable are shown in more detail in Figure 10.

3.2 Generation of single-helicity distributions

In order to perform measurements of the helicity fractions in the ten data samples, it is necessary to know what the distributions of detector measurements would be if the Ws were produced exclusively in each of the three helicities, as per Section 1.3. These distributions are meant to represent the probability densities of the various measurements, not the results of a specific experiment like the simulated data samples. In principle, such distributions could have been obtained in the same manner as the simulated data, but using "reprogrammed" W helicities and much larger Monte Carlo samples. However, that procedure was impractical, owing to the difficulty in reprogramming HERWIG to make single-helicity Ws[12] and the finite amount of disk space available for storing the data. Instead, the data samples themselves are used to calculate the single-helicity distributions, which will be called "template" distributions.

The ten data samples are combined, and muons originating directly from W decay are weighted by the following value for each of the three helicities, where i is the index of the

[11] Integrated luminosity is an effective density of beam particles, measured per unit of transverse area at a collision point in the accelerator. 1 fb = 10^{-39} cm^2.

[12] The difficulty was not associated with modifying the HERWIG Fortran code, but with the re-integration of that modified code into a C++ framework.

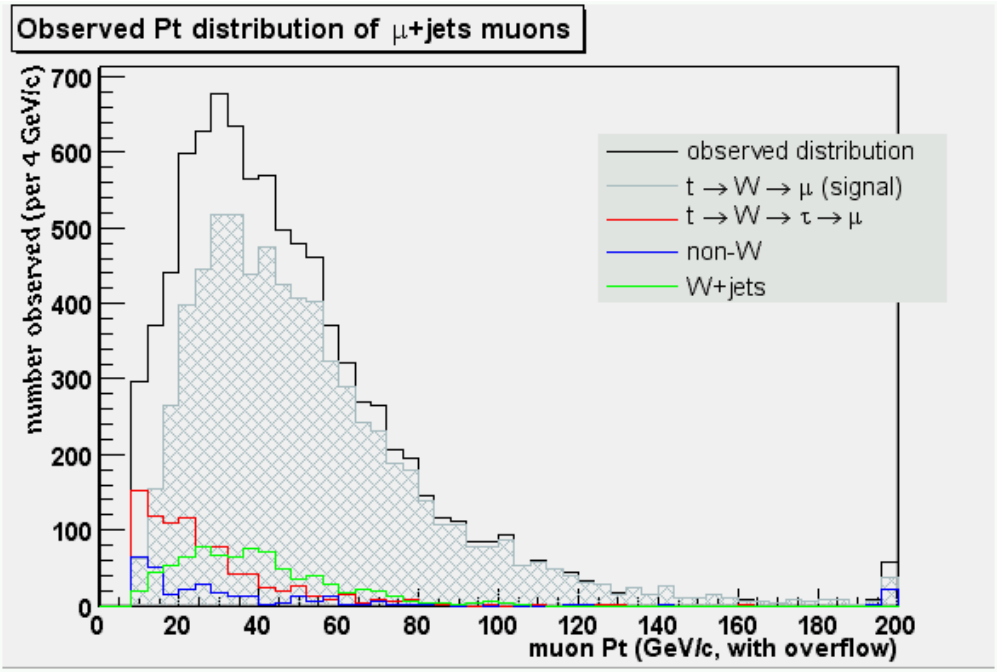

Figure 9: Composition of the P_T distribution for all ten samples combined.

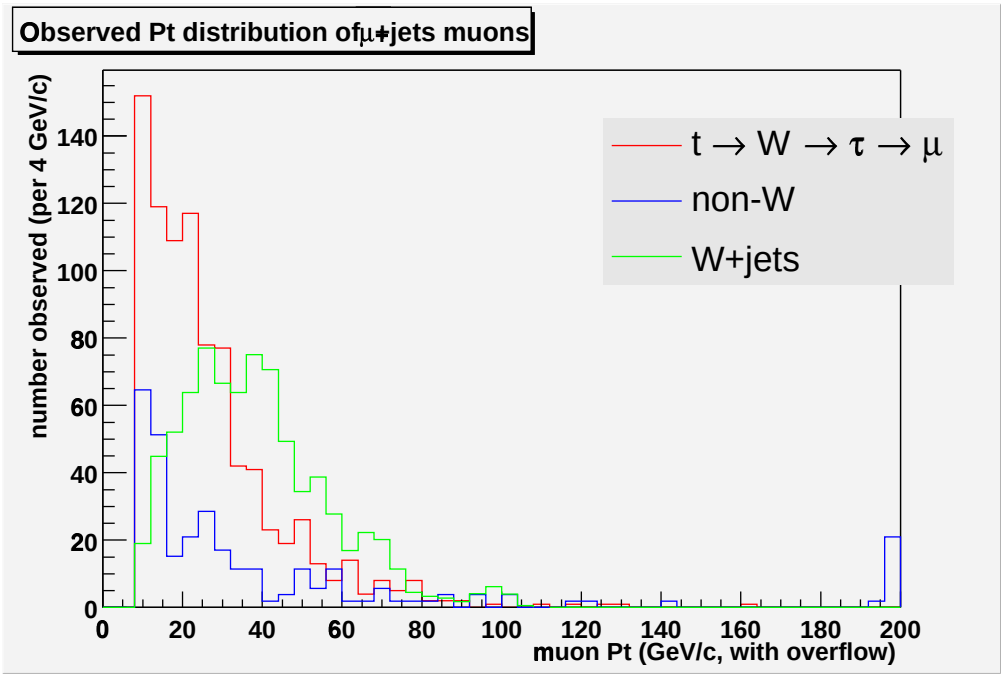

Figure 10: Contributions to the combined muon P_T distribution from each of the three backgrounds.

muon and α_i is that muon's polar decay angle from Figure 2:

$$w_{i,+/0/-} = \frac{\frac{d\mathcal{P}_{+/0/-}}{d(\cos\alpha)}(\cos\alpha_i)}{\left[0.000 \cdot \frac{d\mathcal{P}_+}{d(\cos\alpha)}(\cos\alpha_i)\right] + \left[0.703 \cdot \frac{d\mathcal{P}_0}{d(\cos\alpha)}(\cos\alpha_i)\right] + \left[0.297 \cdot \frac{d\mathcal{P}_-}{d(\cos\alpha)}(\cos\alpha_i)\right]} \quad (5)$$

For the case of muons that decayed from a τ lepton, to be discussed in more detail in Section 5.3, the polar decay angle of the τ is used.

The numerator of Equation (5) is any of the three Equations (3) evaluated at $\cos\alpha_i$, and the denominator is Equation (4), also evaluated at $\cos\alpha_i$, with the Standard Model fractions that are used to generate the data. (Using $m_t = 175$ GeV/c^2 instead of 174.3 GeV/c^2 slightly changes the fractions from Equations (2).) Application of the weight reshapes the decay angle distribution to match those of single-helicity Ws, and modifies the distributions of other helicity-sensitive variables accordingly. The distributions for the (+) helicity produced in this manner display much more statistical jitter than the other two because that state was not originally represented in the data. Those distributions are smoothed in intermediate ranges of the variables. The effects of the re-weighting and smoothing are illustrated for the variable P_T in Figures 11 and 12.

3.3 Mathematical fitting routine used to perform the measurement

The "best fit" of Section 1.3 is performed using a Poisson loglikelihood calculation. Both the "measured" variable distributions of the ten sample sets and the "calculated" variable distributions of the template sets are defined as histograms like the ones used in previous figures. The likelihood, defined independently for each histogram as a function of f_0 and f_-, is a quantity related to the probability that a particular measured histogram was generated by physics obeying a candidate superposition (f_0, f_-) of template distributions. The best fit is the superposition with the greatest likelihood. In this calculation, any given candidate superposition is automatically renormalized to match the number of events in the measured histogram.

For a histogram bin i with with measured value n_i and candidate superposition distribution value $M_i(f_0, f_-)$, the Poisson likelihood, $\mathcal{L}_i$, of the candidate bin is the probability of

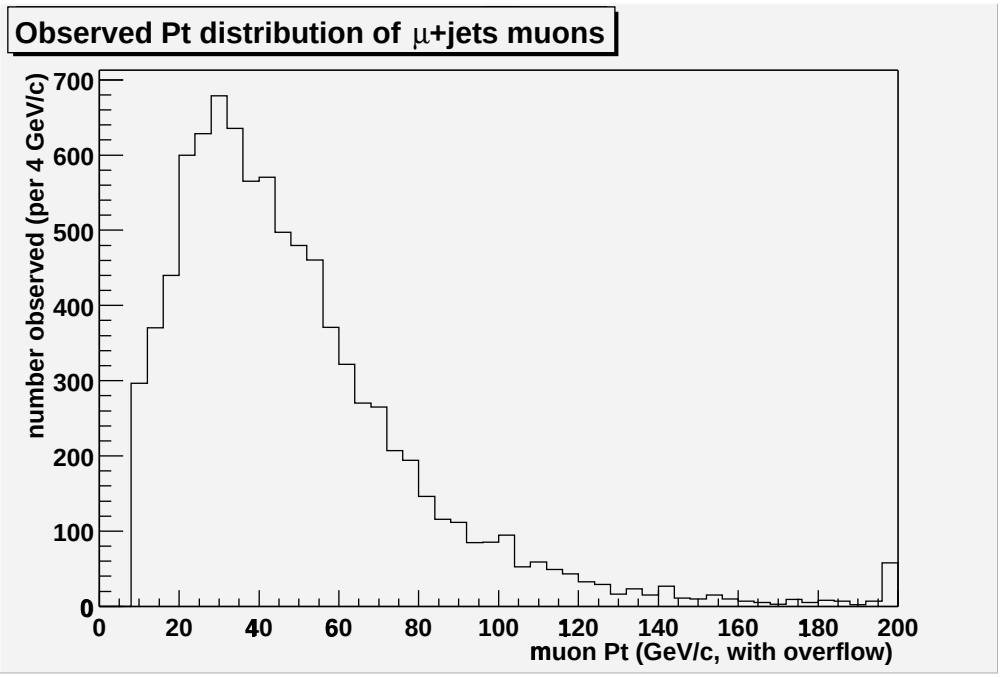

Figure 11: P_T distribution for all ten samples combined.

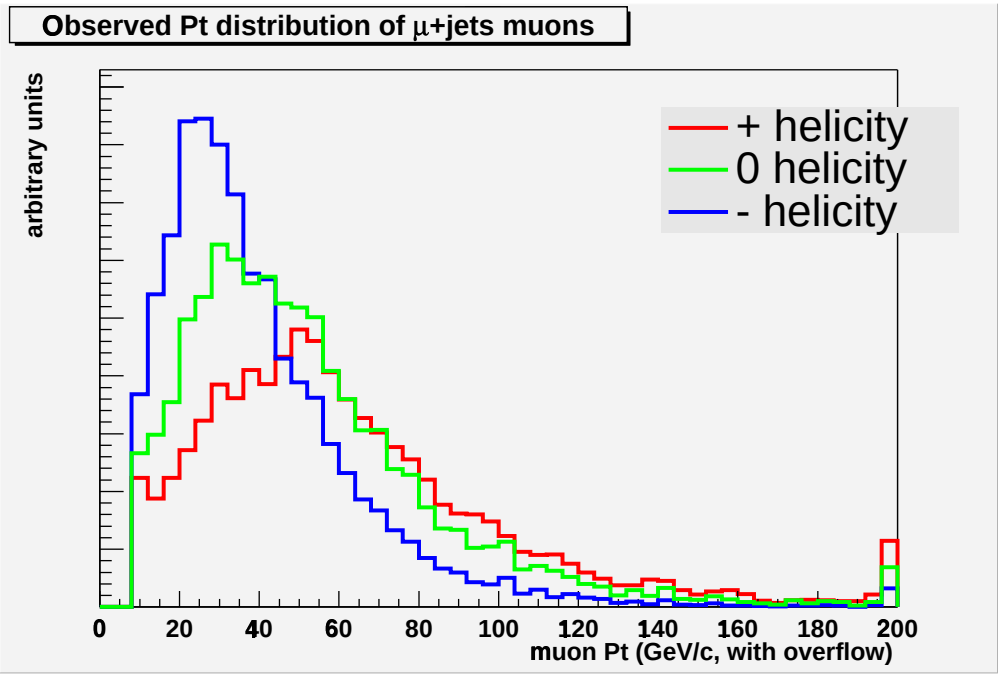

Figure 12: Calculated P_T distributions in the single-helicity cases.

observing n_i with M_i as it's expectation value.

$$\mathcal{L}_i(f_0, f_-) = \frac{[M_i(f_0, f_-)]^{n_i} \cdot e^{-M_i(f_0, f_-)}}{n_i!}. \tag{6}$$

The likelihood, $\mathcal{L}$, of the entire histogram is the product over bins

$$\mathcal{L}(f_0, f_-) = \prod_i \mathcal{L}_i(f_0, f_-). \tag{7}$$

The actual procedure used to find the best fit is to find the minimum value of -2ln $\mathcal{L}(f_0, f_-)$ over the (f_0, f_-) phase space using the MINUIT minimization package [12]. Figure 13 displays an example of such a fit performed on one of the sample P_T distributions.

The 1σ statistical error region of a loglikelihood fit consists of all points in the phase space where the value of -2ln $\mathcal{L}$ departs no more than 1 from the minimum, as shown in Figure 14 for the same example. The error for the two fractions are the respective projections of the 1σ error region onto the two axes. The error for f_+ is calculated using the error correlation coefficient between the two free parameters, ρ_{0-}, which is related to the amount that the 1σ region is tilted with respect to the axes.

$$[\Delta_{stat} f_+]^2 = [\Delta_{stat} f_0]^2 + [2\rho_{0-} \cdot \Delta_{stat} f_0 \cdot \Delta_{stat} f_-] + [\Delta_{stat} f_-]^2 \tag{8}$$

As a more sensitive probe of the parity asymmetry of the W under the assumption that the f_0 prediction is correct, this type of fit is also performed with f_0 fixed to the Standard Model value (with $m_t = 175$ GeV/c^2) of 0.703. The loglikelihood becomes a function only of f_-, and its error region is reduced to the intersection of the 2-parameter error region of Figure 14 with the line $f_0 = 0.703$. This is the same type of measurement that was performed in Run I. Of course, some physics must be assumed in fixing f_0, but it turns out that its value is unchanged for the most natural forms of "new" interactions that could remove maximal parity violation.[13]

[13] All known fundamental interactions involving fermions occur via "vector" and "axial" couplings between the fermions and force-carriers. The only way to change the theoretical value of f_0 is to introduce more complicated forms of interactions. (The hypothetical Higgs mechanism for mass generation introduces "scalar" interactions, but these would produce no new helicity effects.)

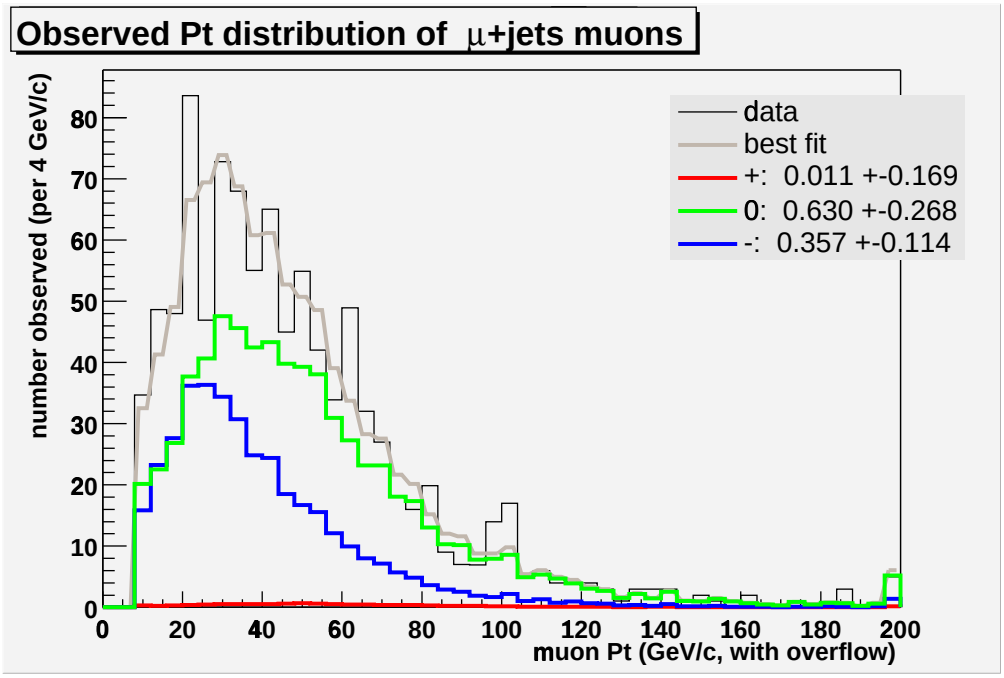

Figure 13: Result of a loglikelihood fit on muon P_T for sample #1.

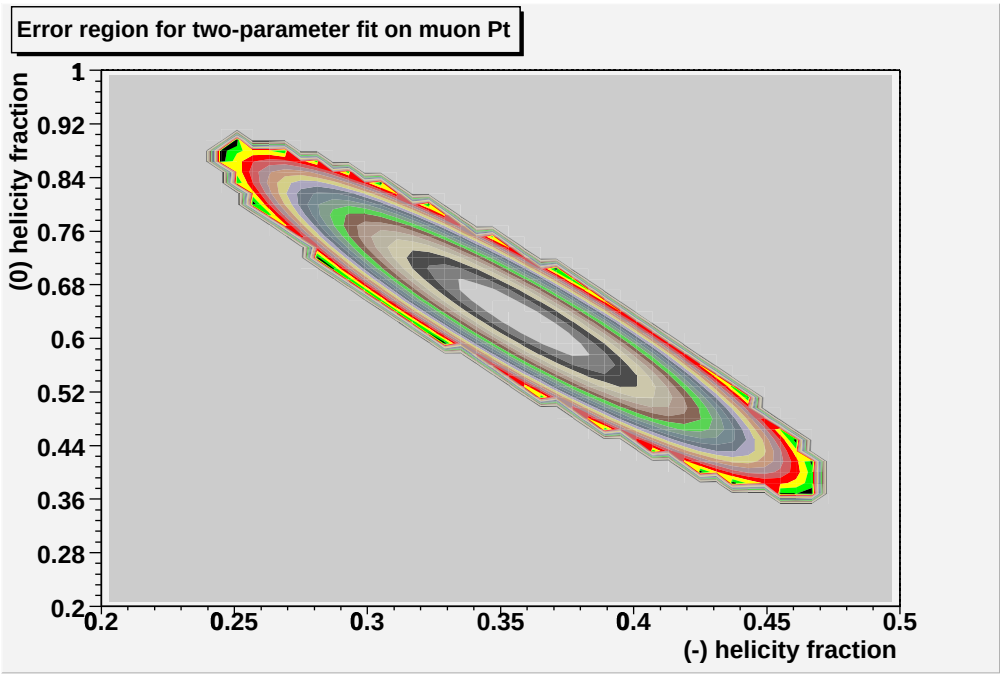

Figure 14: Error region of the fit of Figure 13. The different colors represent rough contours of constant -2ln $\mathcal{L}$. The location of the center, where -2ln $\mathcal{L}$ is minimized, gives the most probable values of f_0 and f_-.

4 Fit Errors

4.1 Sources of statistical error

The shapes and dimensions of fit error regions like the one in Figure 14 are determined by several factors. The simplest of these is just the size of the data set used to make a given histogram. Performing an experiment with N times as much data will scale the errors by $\frac{1}{\sqrt{N}}$. The origin of all other characteristics of the error regions can be qualitatively summed up in the "distinguishability" of the template distributions used in each of the fits, such as the ones shown in Figure 12 for the muon P_T variable. The more dissimilar the three distributions are, the easier it is to discern their individual presences in the data, and the lower the error on their fractions.

In general, the degree of distinguishability present between the template distributions of a given variable varies inversely with the number of and magnitude of uncontrollable factors that come between the W's decay and the laboratory observation. A good example of this effect comes from a comparison of the distributions for the muon polar decay angle (Figure 3) and the distributions for the lab-frame muon momentum (Figure 4), which were discussed in Section 1.3. The former is the most direct variable possible,[14] and shows striking dissimilarities in its distributions. The latter variable's distributions take more effort to distinguish by eye (especially when graphed separately) since they just look like stretched/squashed versions of each other. Here, distinguishability has been lost because the variable is significantly influenced by the velocity of the top quark in the lab frame and the orientation of its decay axis with respect to its trajectory, neither of which take on fixed values for all events. In effect, the influence of the W helicity has been "washed-out" by the underlying randomness of top quark and W boson kinematics, but not so much that the variable cannot be used to perform a measurement.

In an experimental setting, additional error-inducing factors come from the measuring equipment and available identification techniques. In the case of CDF, particle tracks must be reconstructed from detector hits, and jet transverse energy must be reconstructed from calorimeter energy deposits. Neither of these measurements are perfect, since they are in-

[14] In fairness, one can imagine performing a direct measurement of the W helicity with, say, a Stern-Gerlach-type technique, but the W's 10^{-24}s lifetime makes such a measurement practically impossible.

fluenced by inherently unpredictable interactions between the particles and the detector. However, the detector resolution is actually not a large effect for the types of measurements that are addressed by this study. Rather, the presence of backgrounds and the need to impose selection criteria (Section 3.1) are what are most important. As shall be discussed further in Section 4.3, selection criteria can re-shape the template distributions in ways that reduce distinguishability and reduce the overall measurement quality. Without such criteria, though, large amounts of backgrounds in the data and template distributions would lead to even lower quality measurements. Even with selection criteria, the amount of leftover background has a significant influence, accounting for roughly 10-20% of the statistical error of the variables studied here. This is because the background is relatively insensitive to the W helicity (only τ+jets is affected), and consequently contributes a relatively constant underlying presence in the template distributions. Large, constant shifts in the template distributions make them more difficult to distinguish.[15] The influence of detection and identification can be seen by comparing Figures 4 and 15, which, respectively, show the template distributions for the muon momentum before and after detector effects and selection criteria have been taken into account.

4.2 Selection of measurement variables

Each of the above factors can influence the helicity measurement quality of an observable variable in subtle and complex ways. And, on top of these, there are even more factors that induce systematic errors in the measurement procedure itself, which will be addressed in Section 5. Together, they make the task of determining which variables will yield the best helicity measurements into a highly nontrivial one. Nevertheless, this task is actually quite straightforward. The fit procedure described in Section 3 is applied to the simulated data samples for the different variables, and the ones that yield the lowest errors (statistical and systematic combined) are chosen as the "best." These, in turn, can be used to perform the best available measurements when the actual CDF data sample has been accumulated, and, in the meantime, provide error estimates for those measurements.

[15] One can imagine shifting all three distributions upwards by some very large number, at which point all of the W helicity-related features start to look like small-scale statistical jitters.

At this point, two variables have already been introduced: the muon P and P_T. Naturally, muon P_z is a good addition to this set, and, combined with P_T, provides a complete breakdown of the muon's motion (ignoring ϕ, over which there is symmetry). Any extra information useful for the helicity measurement must come from other event variables. Specifically, the only other parts of the event that are related to the W boson that parented the muon are the associated muon neutrino and bottom quark jet. In particular, the invariant mass of the system composed of the bottom quark and the muon has a one-to-one correspondence with the muon's polar decay angle, previously described as the best variable for the helicity measurement. In principle, this can be well-approximated by measuring the bottom jet's momentum and taking its relativistic dot product with the muon's momentum, thereby implicitly accounting for the top quark's motion and significantly reducing its influence a random effect. However, this variable will not be investigated in this study, since proper procedures for identifying bottom quark jets (and their attendant complications) were not addressed.[16] The remaining source of useful information, the neutrino, could not be properly analyzed because of the lack of a realistic $\not\!\!E_T$ measurement. This leaves the muon momentum as the only source of measurement variables for this study.

4.3 Results

The statistical errors on the helicity fractions are now examined using the three muon momentum variables P, P_T, and P_z. Figure 12 from Section 3.3 shows the template distributions for P_T, and Figure 13 shows an example of a fit on that variable. Figures 15 and 16 show the template distributions for P and P_z, and Figures 17 and 18 show examples of fits on those variables. The different degrees of distinguishability discussed in Section 4.1 can once again be seen here, especially between P_z and the other two variables. Each fit is performed for every sample, and the returned fit errors are averaged. The deviation of the error of any given measurement from the mean is usually very small.

For the two-parameter fit, the average statistical errors are

[16] The main complication lies in determining whether a given bottom jet came from t or $\bar{t}$. In other words, which of the two bottom jets came from the same quark as the observed muon?

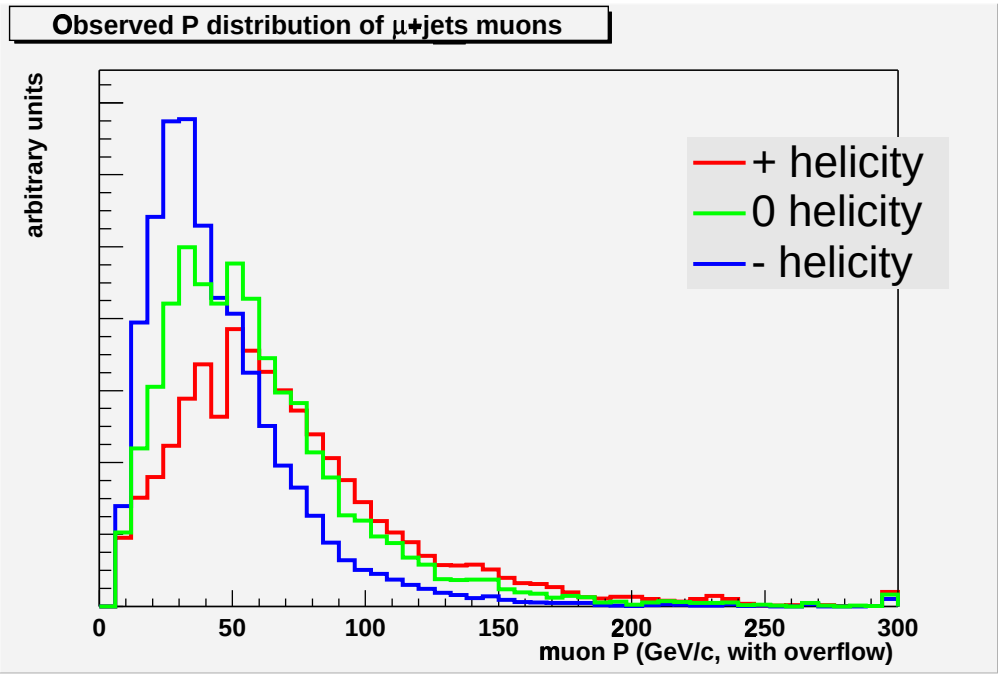

Figure 15: Calculated P distributions in the single-helicity cases.

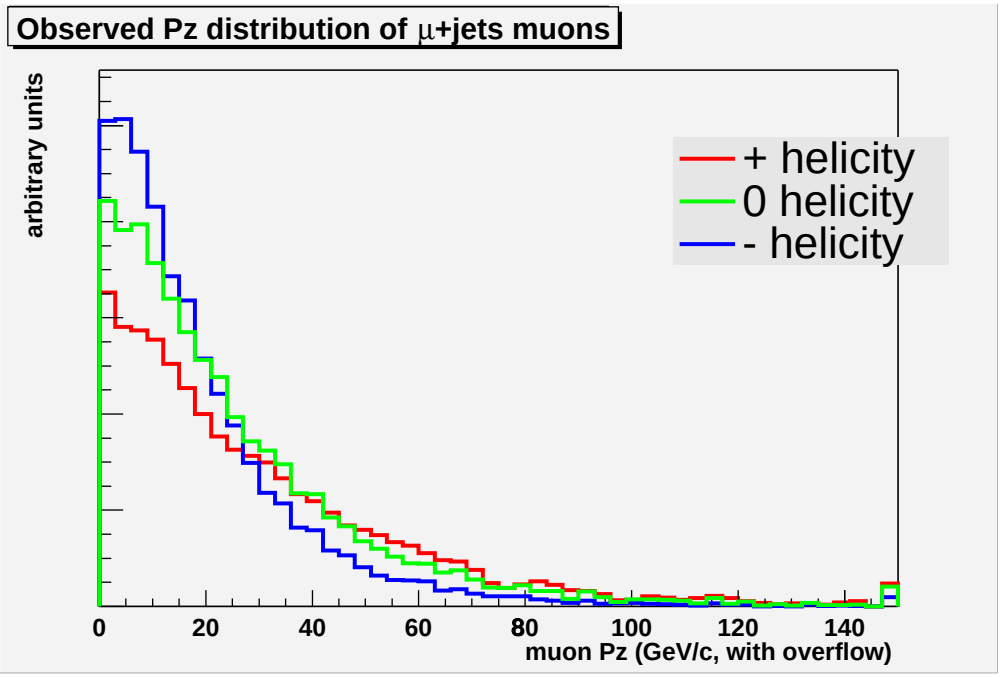

Figure 16: Calculated P_z distributions in the single-helicity cases.

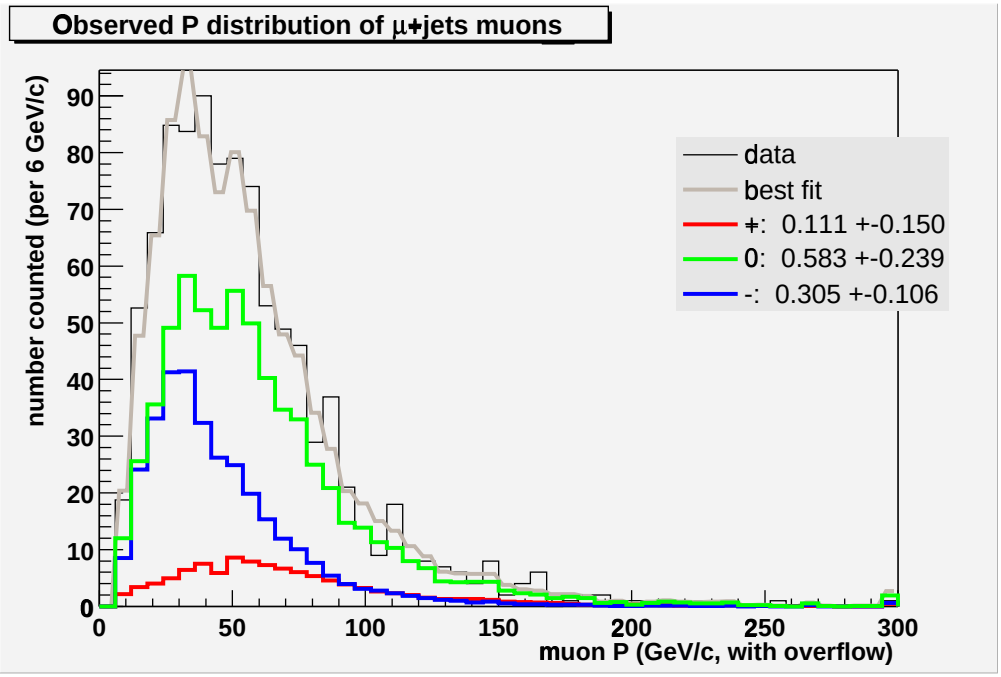

Figure 17: Result of a loglikelihood fit on muon P for sample #4.

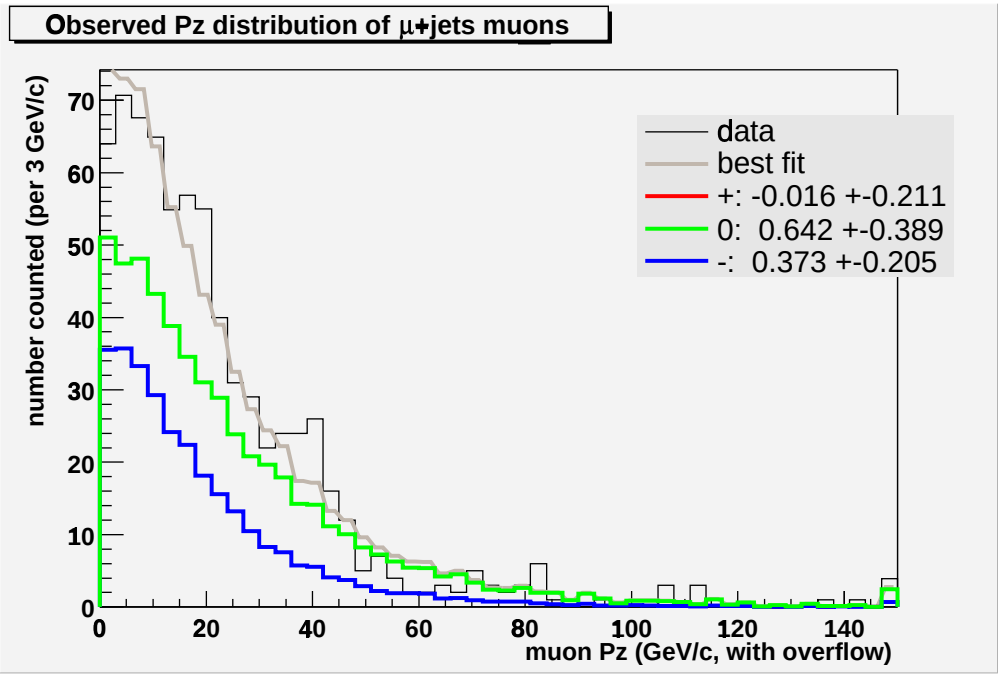

Figure 18: Result of a loglikelihood fit on muon P_z for sample #2.

	$\Delta_{stat} f_+$	$\Delta_{stat} f_0$	$\Delta_{stat} f_-$
P	0.153	0.245	0.111
P_T	0.178	0.286	0.123
P_z	0.233	0.398	0.191

For the one-parameter fit, f_0 is constant and $\Delta_{stat} f_- = \Delta_{stat} f_+$, so only the error on f_+ needs to be listed.

	$\Delta_{stat} f_+$
P	0.0468
P_T	0.0470
P_z	0.0714

P and P_T are shown to be the best of the three variables in terms of minimizing statistical error, with P being marginally better than P_T.

In light of the discussion of Section 4.1, it is interesting to note that there would be a disproportionate decrease in error if there were no need for a $\not\!\!E_T$ cut. To see the effect, fits are performed on background-free data samples with and without the $\not\!\!E_T > 20$ GeV criterion. The removal of backgrounds is necessary because they are explicitly included under the assumption of $\not\!\!E_T > 20$. Of course, the $\not\!\!E_T$ cut is there in the first place to ensure that these backgrounds are small.

Comparison of the two sets of results shows that dropping the cut increases the amount of data going into the histograms by only 13%, but uniformly decreases the errors by around 30% for the (+) and (0) fractions in the two-parameter fits, 10% for the (−) fraction, and 20% for the one-parameter fits (as compared to a predicted 6% reduction in all errors from simple $\frac{1}{\sqrt{N}}$ scaling). The reason for the large error reductions is the fact that the cut is biased against higher-momentum muons, since they tend to be produced with lower-momentum neutrinos as seen in the laboratory frame. The template distributions used for the P_T fits in both studies are shown in Figure 19, illustrating the increase in distinguishability of the distributions at high range when the cut is dropped, especially between (+) and (0).

with $\not\!\!E_T$ cut:

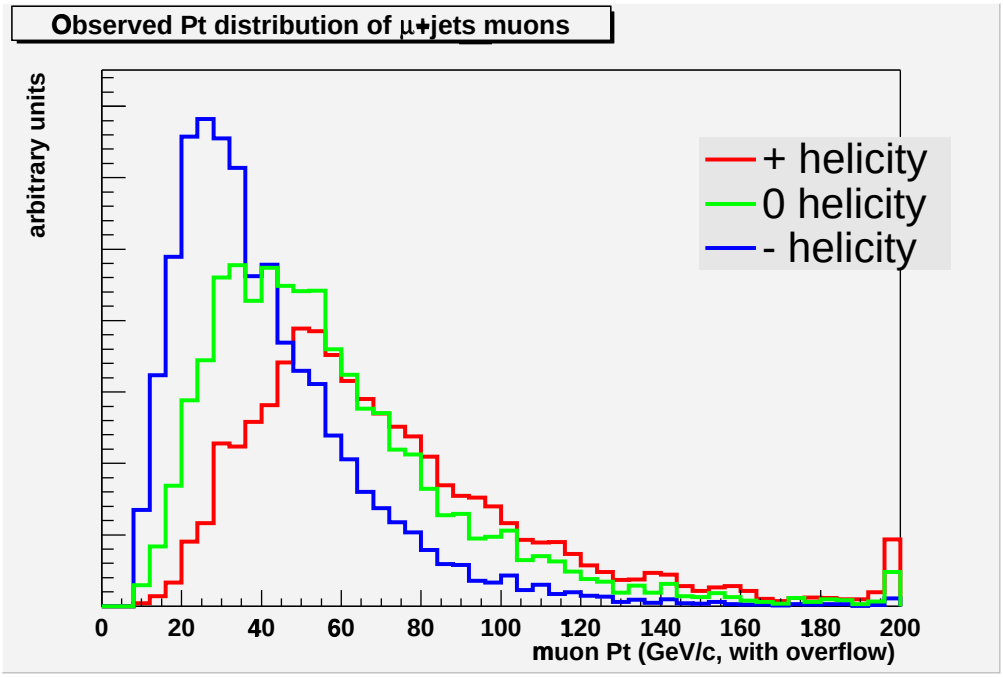

without $\not\!\!E_T$ cut:

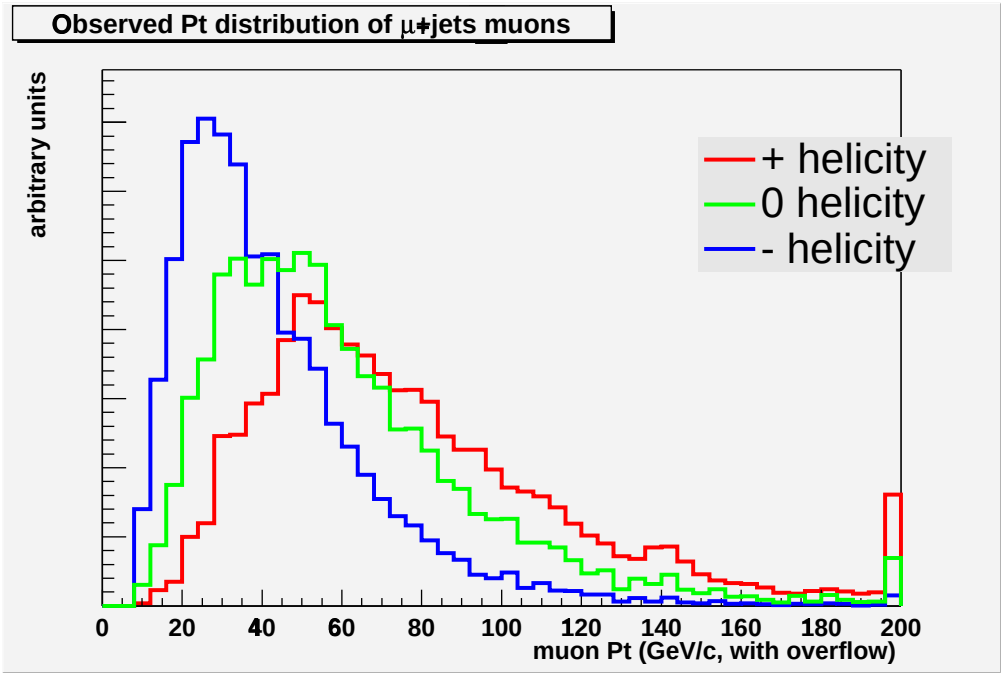

Figure 19: Calculated P_T distributions with and without the $\not\!\!E_T > 20$ GeV criterion, and with no backgrounds.

5 Systematic Errors

5.1 Calculation of systematic errors from backgrounds

The most important systematic errors in the measurement arise from errors in calculating the three backgrounds, predominantly from theoretical uncertainties in the backgrounds' overall rates with respect to μ+jets in the Tevatron. These uncertainties in background rates translate into uncertainties in the appropriate relative normalizations of the background events that are used in construction of the template samples.

To gauge the effects of incorrect normalizations with respect to the data, fits are performed over a range of different normalizations for the individual backgrounds in the template samples. The procedure creates systematic shifts in the returned fit values that vary linearly with the value of the new normalization. The effect can be characterized by its slope, which is obtained by a simple linear fit. Figure 20 shows the systematic change in an average fit value of f_+ versus the strength of the W+jets background relative to the original simulation. The systematic errors in the helicity fractions are the slopes of such plots multiplied by the fractional error in the background normalization.

5.2 Errors from the non-W and W+jets background normalizations

At present, the Run II normalization errors for the non-W and W+jets background are unknown. Because the difficulty associated with making calculations for processes that involve the strong force, the contributions of these two backgrounds can be calculated only after Run II data is accumulated. The errors on those calculations will depend on that data, so at present the only way to determine the systematic errors is to make an educated guess based on the Run I experience: 20% for non-W and 30% for W+jets. These will be used in what follows.

The errors from normalization of the non-W background are listed below.

		$\Delta_{non-W} f_+$	$\Delta_{non-W} f_0$	$\Delta_{non-W} f_-$
two-parameter:	P	0.012	0.026	0.015
	P_T	0.023	0.043	0.020
	P_z	0.007	0.017	0.095

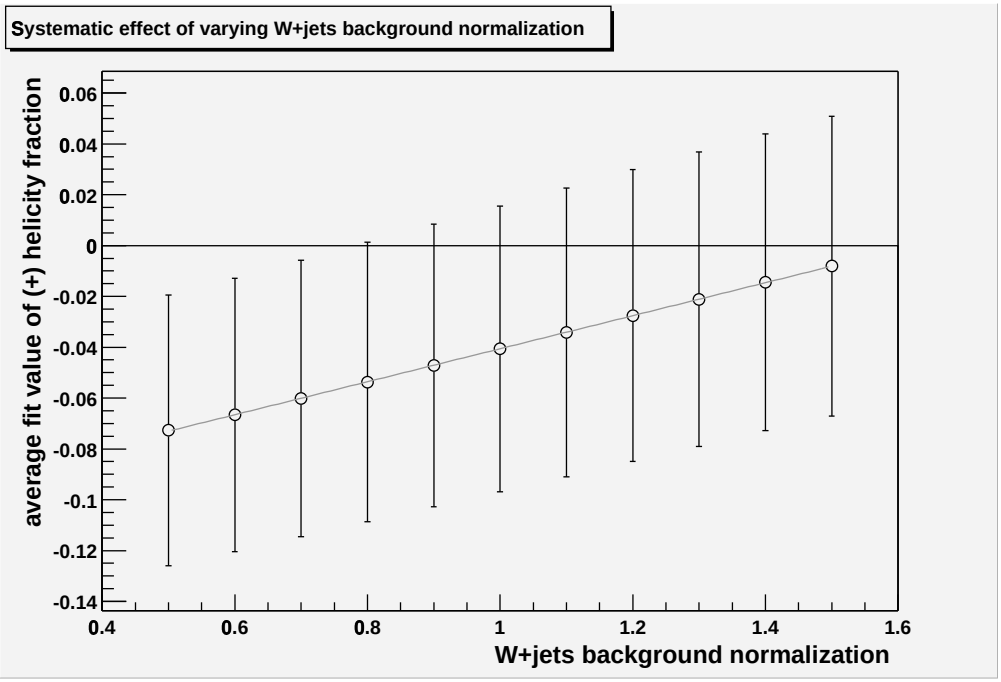

Figure 20: Plot of the systematic effect of the W+jets background normalization on the average measured f_+ in the two-parameter fit on muon P_T. The fact that the graph does not intercept $f_+ = 0$ at relative normalization of 1 is consistent with the statistical error of $\frac{0.18}{\sqrt{10}} = 0.056$ on the average value from the ten samples. The error bars on the different data points are almost completely correlated, allowing for an unambiguous determination of the slope.

		$\Delta_{non-W} f_+$
one-parameter:	P	0.0037
	P_T	0.0029
	P_z	0.0024

And the analogous values for the W+jets background are

		$\Delta_{W+jets} f_+$	$\Delta_{W+jets} f_0$	$\Delta_{W+jets} f_-$
two-parameter:	P	0.012	0.002	0.010
	P_T	0.020	0.011	0.008
	P_z	0.008	0.004	0.004

		$\Delta_{W+jets} f_+$
one-parameter:	P	0.0102
	P_T	0.0128
	P_z	0.0057

5.3 Errors from the τ background

The normalization of the background from τ+jets is much better known because it depends on the ratio between the probabilities of $W \to \tau\nu_\tau$ and $W \to \mu\nu_\mu$ decays, which has been measured with 3.3% error[17] [7]. However, the relatively large contribution of τ+jets to the data sets makes this small uncertainty into a non-negligible source of systematic error. Those errors are

		$\Delta_{\tau+jets} f_+$	$\Delta_{\tau+jets} f_0$	$\Delta_{\tau+jets} f_-$
two-parameter:	P	0.006	0.015	0.009
	P_T	0.006	0.016	0.009
	P_z	0.001	0.008	0.007

		$\Delta_{\tau+jets} f_+$
one-parameter:	P	0.0030
	P_T	0.0032
	P_z	0.0032

The fact that the relatively massive τ is influenced by the physics of Ws produced in top decay opens the possibility of some unknown mass-related behavior that alters the *shape* of the τ+jets contributions to the variable distributions but leaves the contributions from actual μ+jets unaffected. Though this type of scenario is very unlikely, an extra study is performed with an extreme change in the physics of the $W \to \tau\nu_\tau$ process to test whether an

[17] Theoretically, this ratio is unity. This is consistent with the measured value 1.016 ± 0.033.

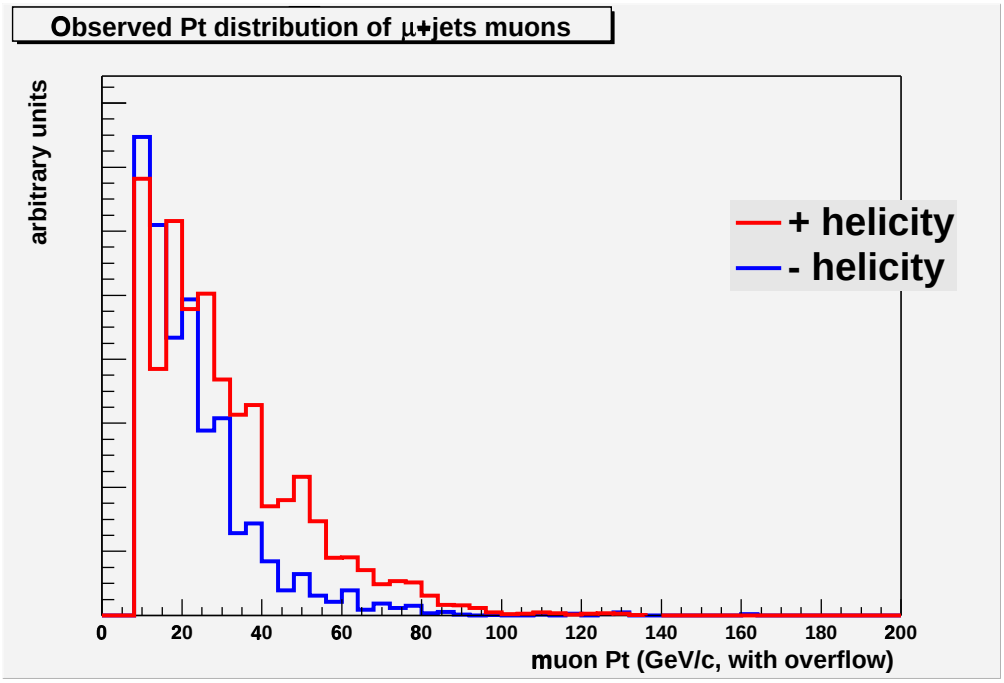

Figure 21: Normal contributions to the calculated (+) and (−) helicity distributions from τ+jets muons. For sense of scale, the peaks on the left are about $\frac{1}{6}$th the height of the peak of the (−) distribution in Figure 12.

effect would be seen. As with the normalization studies, the background is left untouched in the data samples, but now the template distributions are constructed under the assumption that the sign of the helicity of the W's decay products in Figure 2 is reversed when the W decays into τ. In other words, the "wrong-signed" version of Equation (5) is used on the muons from τ decay for the (+) and (−) distributions. The distinction between the τ+jets background contributions in the two cases is shown in Figure 21. For the two-parameter fit on P_T, the result is a +0.028 shift in the average measured f_+ and a -0.047 shift in the average measured f_0. The shifts for the other two-parameter fits are similarly a couple of times larger than the respective systematic errors from τ+jets normalization. The shifts for the one-parameter fits are more on par with their corresponding τ+jets errors or are smaller than them. For P_T again, the shift in f_+ is only +0.0001, but for P the shift is +0.0014. The point here is not to include these as errors in the final results, but to note that unusual τ physics can have an influence on the fit results that is greater than the errors from τ+jets normalization, and that those results cannot be considered insensitive to such physics

when the normalization-based errors are significant. (This statement remains true when the stricter selection criteria of Section 6 are used.) For the simulated data sets analyzed here, statistical errors alone vastly dominate any potential effects from anomalous τ physics. Such effects could only be significant for data sets that are several times larger.

5.4 Other sources of systematic error

In addition to background normalization, there are a variety of other factors that introduce uncertainty into the construction of the template samples. They include uncertainties in the background distribution shapes, in the top quark mass, in the effects of strong force radiative processes, and in the distribution of quarks and gluons inside of the protons and antiprotons that are collided in the Tevatron. These factors were not studied here due to the difficulty of accurately determining their influence. However, their contribution to the total measurement error is expected to be small compared to the combined effect from the background normalizations. This expectation is supported by the contributions calculated for the Run I one-parameter measurement of f_0 (reference [9]), for which the quadrature sum of the errors from non-W background shape, a conservatively rescaled top quark mass uncertainty,[18] strong force radiation, and quark/gluon distribution is slightly larger than the error from non-W normalization alone.

6 Total Errors

6.1 Selection criteria and measurement optimization

The event selection criteria used to define a data set represent the single factor affecting the helicity measurement error that is under the experimentalist's control after data has been accumulated. Though the criteria listed in Section 3.1 were designed for large acceptance of the μ+jets signal and small acceptance of the background, there remains the possibility that those criteria are not ideal, and should be changed in order to obtain the best measurement possible. In making such alterations, there are two main competing effects. For example, strengthening the criteria allows less actual μ+jets events into the data sample, thereby

[18] The top quark mass uncertainty is scaled to 3.0 GeV/c^2 from 5.1 GeV/c^2 to represent a possible Run II refinement.

tending to increase the statistical error. However, this also allows less background into the sample, thereby tending to decrease the systematic errors and the background's effect on the statistical errors. Similarly, the opposite effects occur when the selection criteria are loosened. The question, then, is whether the measurement improvement associated with a change in criteria is larger than the measurement degradation, and the goal is to find and use the set of criteria where any change yields larger total errors.

With the full direct lepton sample, there will be three different sets of selection criteria which must be individually optimized; one each for μ+jets, e+jets, and dilepton event samples. Since this study only addresses μ+jets, optimization of that subsample alone will be pursued in what follows. These optimized results will then be offered as the Run II helicity measurement error estimates.

6.2 Conservative sample (1,000 events)

The statistical and systematic errors calculated in the previous two sections are combined by quadrature sum to yield the total errors for the three muon momentum variables under the default μ+jets selection criteria:

		$\Delta_{total} f_+$	$\Delta_{total} f_0$	$\Delta_{total} f_-$
two-parameter:	P	0.154	0.247	0.112
	P_T	0.181	0.290	0.126
	P_z	0.234	0.398	0.191

		$\Delta_{total} f_+$
one-parameter:	P	0.0482
	P_T	0.0489
	P_z	0.0718

These errors differ by at most a few percent from the statistical errors tabulated in Section 4.3. Consequently, even if it were possible to modify the selection criteria to preserve all of the real events and eliminate all of the background events, the improvement of the error would be minuscule. Indeed, strengthening of the minimum P_T and maximum $|\eta|$ criteria show uniform increases in total errors associated with decreased statistics. Loosening the P_T criterion, on the other hand, introduces no new real μ+jets events in any of the samples (only new background), and loosening the maximum $|\eta|$ criterion has absolutely no effect,

since it was implemented implicitly by the muon detector coverage. Effects of altering the other selection criteria are not explored here, but their application is based on a large body of CDF experience in maximizing measurement quality in Run I.

Since very little can be accomplished from trying to optimize the above set of measurement errors, the best errors from that set will be used as-is for the final estimated measurement errors on the approximately 1,000 direct leptons expected from the first stage of Run II. Those best errors belong to P for both the one- and two-parameter measurements, making the final estimates:

	$\frac{\Delta_{total} f_+}{0.154}$	$\frac{\Delta_{total} f_0}{0.247}$	$\frac{\Delta_{total} f_-}{0.112}$
two-parameter:			

	$\frac{\Delta_{total} f_+}{0.0482}$
one-parameter:	

6.3 Anticipated final sample (10,000 events)

The full length of Run II is predicted to see at least a tenfold increase in data over the first stage. This translates to a $\frac{1}{\sqrt{10}}$ scaling of the statistical errors in the W helicity measurement, leading to the following total errors with the default μ+jets selection criteria:

		$\frac{\Delta_{total} f_+}{0.052}$	$\frac{\Delta_{total} f_0}{0.083}$	$\frac{\Delta_{total} f_-}{0.040}$
two-parameter:	P			
	P_T	0.064	0.102	0.046
	P_z	0.075	0.127	0.062

		$\frac{\Delta_{total} f_+}{0.0186}$
one-parameter:	P	
	P_T	0.0201
	P_z	0.0237

Here, the total errors are more like 10-20% greater than the statistical errors alone, making the search for ideal selection criteria less futile than it was with the conservative sample. To determine the ideal minimum P_T criterion, that criterion is varied from "$P_T > 8$ GeV/c" to "$P_T > 24$ GeV/c" in increments of 4 GeV/c, and all errors are recalculated for each increment. P remains the best variable throughout this investigation, so its results alone are listed.

two-parameter:

min. P_T	$\Delta_{total} f_+$	$\Delta_{total} f_0$	$\Delta_{total} f_-$
08	0.0516	0.0831	0.0401
12	0.0507	0.0814	0.0388
16	0.0557	0.0910	0.0429
20	0.0587	0.1001	0.0490
24	0.0573	0.1042	0.0551

one-parameter:

min. P_T	$\Delta_{total} f_+$
08	0.0186
12	0.0186
16	0.0184
20	0.0166
24	0.0176

The individual statistical and systematic errors under the different minimum P_T criteria are tabulated in the appendix.

Variation of the $|\eta|$ criterion (with $P_T > 8$ GeV/c) from "$|\eta| < 1.2$" to "$|\eta| < 0.9$" in increments of 0.1 causes the statistical errors to increase by up to 5% with no significant changes in systematic errors. Consequently, the default $|\eta|$ will not be altered.

The difference between the errors obtained with the default $P_T/|\eta|$ criteria and the ideal $P_T/|\eta|$ criteria are 1-3% for the two-parameter and 10% for the one-parameter. Thus, only the one-parameter measurement displays even a remotely significant improvement.

The best errors for the 10,000-event extrapolation are listed below, with P as the fit variable and $P_T > 12$ GeV/c for the two-parameter measurement and $P_T > 20$ for the one-parameter measurement:

two-parameter:

$\Delta_{total} f_+$	$\Delta_{total} f_0$	$\Delta_{total} f_-$
0.0507	0.0814	0.0388

one-parameter:

$\Delta_{total} f_+$
0.0166

7 Conclusions

The estimates calculated in the previous section display, as expected, a large improvement over the Run I measurements. The two-parameter measurement, which formerly yielded no

results, will at least match the Run I one-parameter measurement of f_+ by the end of the first stage of Run II, and will improve upon the one-parameter measurement of f_0 with at least a 40% error reduction. By the end of Run II, the one-parameter measurement of f_+ will probably be able to probe for an anomalous departure from maximal parity violation at the scale of a couple percent, with the assumption of no highly unorthodox new physics.

More accurate estimates will require full investigation of the errors associated with e+jets and dilepton events, of the utility of the b jet and $\not\!\!E_T$ data, and/or of the contributions from the additional systematics discussed in Section 5.4. After accounting for all of these, it is quite likely that the estimated measurement quality will display further improvements. In addition, of course, such estimates will also benefit from more accurate values for the overall size of the data sample and the errors on the non-W and W+jets background normalizations, which will both be refined as CDF takes data over the next several years. These refinements can be directly applied to the results of this study by simple rescaling of the errors listed in the appendix, which then provides an immediate guide to optimizing the minimum P_T criterion for the μ+jets subsample in the 8 GeV/c to 24 GeV/c region (lacking the b jet and $\not\!\!E_T$ detector data).

A Tabulation of individual errors from section 6.3

This appendix contains the individual statistical and systematic errors associated with the one- and two-parameter fits on P with the five lower bounds on P_T, as used to calculate the total errors on a 10,000-event sample in Section 6.3.

two-parameter

f_+:

min. P_T	Δ_{stat}	Δ_{non-W}	Δ_{W+jets}	$\Delta_{\tau+jets}$
08	0.0485	0.0119	0.0115	0.0056
12	0.0495	0.0060	0.0088	0.0036
16	0.0546	0.0014	0.0106	0.0026
20	0.0580	0.0023	0.0086	0.0015
24	0.0568	0.0033	0.0068	0.0004

f_0:

min. P_T	Δ_{stat}	Δ_{non-W}	Δ_{W+jets}	$\Delta_{\tau+jets}$
08	0.0774	0.0265	0.0020	0.0147
12	0.0792	0.0148	0.0030	0.0109
16	0.0905	0.0045	0.0009	0.0060
20	0.0996	0.0062	0.0037	0.0062
24	0.1036	0.0079	0.0084	0.0036

f_-:

min. P_T	Δ_{stat}	Δ_{non-W}	Δ_{W+jets}	$\Delta_{\tau+jets}$
08	0.0349	0.0146	0.0096	0.0056
12	0.0352	0.0088	0.0118	0.0073
16	0.0412	0.0032	0.0097	0.0060
20	0.0470	0.0039	0.0124	0.0005
24	0.0528	0.0048	0.0152	0.0032

one-parameter

f_+:

min. P_T	Δ_{stat}	Δ_{non-W}	Δ_{W+jets}	$\Delta_{\tau+jets}$
08	0.0148	0.0037	0.0102	0.0030
12	0.0149	0.0027	0.0104	0.0027
16	0.0153	0.0012	0.0100	0.0022
20	0.0161	0.0011	0.0034	0.0014
24	0.0175	0.0011	0.0011	0.0014

Acknowledgments

This paper and its author owe a large debt of gratitude to Prof. Kevin McFarland. Kevin took me on as a summer student at the end of my sophomore year, giving me an unsuspected alternative to my initial choice between a summer of complete idleness or a "real" job. Working on this project with him over the past two years has been an equally unsuspected pleasure. Through his patient guidance, I have learned more than I am sure I even currently realize, and see my future path in life with a view far clearer than any undergraduate coursework could have granted me.

Kevin's group at CDF has also been instrumental in my learning process. Kirsten Tollefson in particular was of great help during my first weeks at CDF. Ben Kilminster, Tony Vaiciulis, Sarah Demers, Mike Carew, Jedong Lee, Erika Artukovik, Han Yoo, and Wells Wulsin (in no particular order) have all served as invaluable allies in my constant struggle to make the CDF software do what I wanted, and provided the ears necessary for me to brag about when it actually did.

My undergraduate colleagues Andrew Blechman and Albert Wang deserve a measure of recognition for this document as well. Andrew has served as a sounding board for many of my ideas on high energy physics and life in general. His friendship, his passion for physics, and his culinary generosity have provided a not-insubstantial part of my motivation for completing this work and staying in this field. Albert works on condensed matter, so I have no comprehension of what he does or why he does not work in my obviously superior field, and vice versa. However, we have a major common ground in pursuing quality work and mocking each other for it. Albert has been a major force in keeping my work in perspective, especially on those 4am shifts when we were the only two people in the physics building.

Finally, I am indebted to the incredibly helpful University of Rochester physics staff. Specific thanks go to Connie Jones, who has performed countless invaluable secretarial feats for me in the processes of performing and presenting this research. Also, Janet Fogg deserves special mention for several helpful conversations and some lighting-fast duplicating.

References

[1] F. Abe *et al.* [CDF Collaboration], "Observation of Top Quark Production in $\overline{p}p$ Collisions," Phys. Rev. Lett. **74**, 2626 (1995) [hep-ex/9503002].

[2] S. Abachi *et al.* [DØ Collaboration], "Observation of the Top Quark," Phys. Rev. Lett. **74**, 2632 (1995) [hep-ex/9503003].

[3] S. W. Herb *et al.*, "Observation of a Dimuon Resonance at 9.5-GeV in 400-GeV Proton - Nucleus Collisions," Phys. Rev. Lett. **39**, 252 (1977).

[4] M. L. Perl *et al.*, "Evidence for Anomalous Lepton Production in e^+e^- Annihilation," Phys. Rev. Lett. **35**, 1489 (1975).

[5] J. H. Christenson, J. W. Cronin, V. L. Fitch and R. Turlay, "Evidence for the 2π Decay of the K_2^0 Meson," Phys. Rev. Lett. **13**, 138 (1964).

[6] F. J. Gilman and R. Kauffman, "Top Decays when $m_t \approx M_W + m_b$," Phys. Rev. D **37**, 2676 (1988).

[7] D. E. Groom *et al.* [Particle Data Group Collaboration], "Review of Particle Physics," Eur. Phys. J. C **15**, 1 (2000) and 2001 partial update for edition 2002.

[8] G. Mahlon, private communication.

[9] T. Affolder *et al.* [CDF Collaboration], "Measurement of the Helicity of W Bosons in Top Quark Decays," Phys. Rev. Lett. **84**, 216 (2000) [hep-ex/9909042].

[10] G. Corcella *et al.*, "HERWIG 6: An Event Generator for Hadron Emission Reactions with Interfering Gluons (Including Supersymmetric Processes)," JHEP **0101**, 010 (2001) [hep-ph/0011363].

[11] T. Affolder *et al.* [CDF Collaboration], "Measurement of the Top Quark Mass with the Collider Detector at Fermilab," Phys. Rev. D **63**, 032003 (2001) [hep-ex/0006028].

[12] F. James and M. Roos, "'Minuit' a System for Function Minimization and Analysis of the Parameter Errors and Correlations," Comput. Phys. Commun. **10**, 343 (1975).